

There were a few editorial errors in the appendix of this version of paper, which showed earlier circuit design that has been subsequently changed. A newer version of the paper is forthcoming.

SUPPORTING ENERGY-BASED LEARNING WITH AN ISING MACHINE SUBSTRATE: A CASE STUDY ON RBM

Uday Kumar Reddy Vengalam, University of Rochester, USA, uvengala@ur.rochester.edu¹
Yongchao Liu, University of Rochester, USA, yliu234@ur.rochester.edu¹
Tong Geng, University of Rochester, USA, tong.geng@rochester.edu¹
Hui Wu, University of Rochester, USA, hui.wu@rochester.edu¹
Michael Huang, University of Rochester, USA, michael.huang@rochester.edu¹

ABSTRACT

Nature apparently does a lot of computation constantly. If we can harness some of that computation at an appropriate level, we can potentially perform certain type of computation (much) faster and more efficiently than we can do with a von Neumann computer. Indeed, many powerful algorithms are inspired by nature and are thus prime candidates for nature-based computation. One particular branch of this effort that has seen some recent rapid advances is Ising machines. Some Ising machines are already showing better performance and energy efficiency for optimization problems. Through design iterations and co-evolution between hardware and algorithm, we expect more benefits from nature-based computing systems. In this paper, we make a case for an augmented Ising machine suitable for both training and inference using an energy-based machine learning algorithm. We show that with a small change, the Ising substrate accelerate key parts of the algorithm and achieve non-trivial speedup and efficiency gain. With a more substantial change, we can turn the machine into a self-sufficient gradient follower to virtually complete training entirely in hardware. This can bring about 29x speedup and about 1000x reduction in energy compared to a Tensor Processing Unit (TPU) host.

1 INTRODUCTION

Nature apparently does a lot of computation all the time, solving differential equations, performing random sampling, and so on. We have harnessed some of it of course. The transistors, for example, can be turned on and off based on the law of nature. They are practically the foundation for most of our computers today. But this is different from harnessing nature's computational capability at some higher level, for example, to solve an entire problem. Indeed, some very powerful algorithms are inspired by nature (Zames et al., 1981; Kirkpatrick et al., 1983; Ackley et al., 1985). It is not hard to imagine that if a computing substrate is nature-based we could solve a certain set of problems much more quickly and efficiently than through mapping it to the von Neumann interface.

Among various critical real-world problems, Machine Learning (ML) training is known to be extremely computationally expensive¹, which calls for a breakthrough solution to reduce the computational time and energy cost. We believe that a nature-based computing substrate could provide

a potential fundamental solution to this issue. This idea is actually not entirely new – recently, Hinton has discussed a similar perspective in (Hinton, 2022). Specifically, he emphasized the significance of utilizing the nature of electronic components (such as capacitors, resistors, and conductors) in analog hardware to enable efficient ML with mortal computation. However, he also acknowledged that implementing backpropagation using nature-based computing substrates, as opposed to forward propagation, is a significant challenge.

This motivates us to investigate whether the recent emerging high-performance nature-based computing substrates have the potential for efficient ML. One particular branch of such computing substrates that has seen some recent rapid advances is Ising machines. In a nutshell, Ising machines leverage nature to seek low energy states for a system of coupled spins. A number of problems (in fact, all NP-complete problems) can be expressed as an equivalent optimization problem of the Ising formula (more on that in Sec. 2). Though existing Ising machines are largely in the form of prototypes and concepts, they are already showing promise of (much) better performance and energy efficiency for optimization problems. But the real appeal is in

¹ChatGPT is estimated to have cost over 10,000 GPUs in the training and over \$4 million in each training session.

their future opportunities. First, through design iterations, their computational capacity and efficiency will continue to improve, hopefully quickly and significantly as they have in the recent past. Second, with novel hardware, the design of algorithms (especially those inspired by nature) will co-evolve with the hardware and lead to a richer combination of problem-solving modalities.

In this paper, we make a concrete case for this second point by demonstrating that an augmented Ising machine design can bring $29\times$ speedup with $1000\times$ energy cost reduction over TPUs to the training of Restricted Boltzmann Machine (RBM) and variants, a machine learning modality that has drawn considerable attention recently. It is worth noting that Boltzmann-Machine-based ML has emerged as a promising approach for solving various real-world networking problems including recommendation systems (Liu et al., 2023) and traffic prediction (Pan et al., 2023), outperforming traditional neural network solutions in terms of both inference speed and accuracy. However, the training of Boltzmann-Machine-based models remains prohibitively expensive, thus hindering the realization of their full potential in the future. The proposed training approach based on the Ising machine will fundamentally address this problem.

It is also important to note that we believe the true appeal lies in what we can do when we *co-design* the hardware and the algorithm². In this paper, we mostly follow the existing practice in terms of the training algorithm as this is merely the first step of our exploration. In the future, we will investigate how to extend the proposed solution to general ML.

2 BACKGROUND AND RELATED WORK

2.1 Principles of Ising machines

The Ising model is used to describe the Hamiltonian of a system of coupled spins. The spins have one degree of freedom and take one of two values (+1, -1). The energy of the system is a function of pair-wise coupling of the spins (J_{ij}) and the interaction (h_i) of some external field (μ) with each spin. The resulting Hamiltonian is as follows:

$$H = - \sum_{(i<j)} J_{ij} \sigma_i \sigma_j - \mu \sum_i h_i \sigma_i \quad (1)$$

A physical system with such a Hamiltonian naturally tends towards low-energy states. It is as if nature tries to solve an optimization problem with Eq. 1 as the objective function, which is not a trivial task. Indeed, the cardinality of the state space grows exponentially with the number of

spins, and the optimization problem is NP-complete: it is easily convertible to and from a generalized max-cut problem, which is part of the original list of NP-complete problem (Karp, 1972).

Thus if a physical system of spins somehow offers programmable coupling parameters (J_{ij} and μh_i in Eq. 1), they can be used as a special purpose computer to solve³ optimization problems that can be expressed in Ising formula (Eq. 1). In fact, all problems in the Karp NP-complete set have their Ising formula derived (Lucas, 2014). Also, if a problem already has a QUBO (quadratic unconstrained binary optimization) formulation, mapping to Ising formula is as easy as substituting bits for spins: $\sigma_i = 2b_i - 1$.

Because of the broad class of problems that can map to the Ising formula, building nature-based computing systems that solve these problems has attracted significant attention (Kim et al., 2010; Bunyk et al., 2014; Yamaoka et al., 2015; Barends et al., 2016; Berloff et al., 2017; King et al., 2018; Böhm et al., 2019a; Hamerly et al., 2019b; Pierangeli et al., 2019).

It is important to note that different approaches may offer different fundamental tradeoffs and goes through varying gestation speeds. Thus it could be premature to evaluate a general approach based on observed instances of prototypes. Nevertheless, we provide a broad-brushed characterization, which can help researchers get a basic sense of the landscape – as long as the caveats are properly understood.

2.2 The three generations of Ising machines

Some of the earliest and perhaps the best known Ising machines are the quantum annealers marketed by D-Wave. At the moment, quantum annealers are extremely sensitive to noise, necessitating cryogenic operating condition that consumes much power (25KW for D-Wave 2000q). Also, they use a local coupling network, which means the the nominal 2000 nodes on the D-Wave 2000q is equivalent to only about 64 effective nodes (Hamerly et al., 2018; 2019a).

Coherent Ising Machines (CIM) can be thought of as a second-generation design where some of the issues are addressed (Inagaki et al., 2016; McMahan et al., 2016; Takata et al., 2016; Yamamoto et al., 2017; Böhm et al., 2019b). However, besides their own technical challenges, the current CIMs all use computed rather than physical coupling. Such a design will unlikely to be energy-efficient due to fundamental reasons.

Since the operating principle of CIM can be viewed with a Kuramoto model (Takeda et al., 2017), using other oscilla-

²Indeed, having different substrates can create the same type of cross-pollination that led to quantum-inspired algorithms (Narayanan & Moore, 1996).

³Throughout the paper, by “solving” an optimization problem we mean the searching for a good solution rather than finding the global optimum, equivalent to reaching the ground state.

tors can in theory achieve a similar goal. This led to a number of electronic Oscillator-based Ising Machines (OIM) which can be considered as a third-generation. These systems use LC tanks for spins and (programmable) resistors as coupling units. However, for on-chip integration, inductors are often a source of practical challenges. They are area intensive, have undesirable parasitics with reduced quality factor and increased phase noise all of which pose practical challenges in maintaining frequency uniformity and phase synchronicity between thousands of on-chip oscillators.

Another electronic design with a different architecture is the Bistable Resistively-coupled Ising Machine (BRIM) (Afoakwa et al., 2021). In BRIM, the spin is implemented as capacitor voltage controlled by a feedback circuit, making it bistable. The design is CMOS-compatible and since it uses voltage (as opposed to phase) to represent spin, it enables a straightforward interface to additional architectural support for computational tasks. We therefore use a baseline substrate similar to BRIM. Note that the same principle discussed in the paper could directly apply to all Ising machines with different amount of glue logic.

2.3 Energy-based models

The concept of energy is used not only in traditional optimization algorithms (Kirkpatrick et al., 1983) but also in a number of machine learning algorithms collectively referred to as Energy-Based Models (EBM) (LeCun et al., 2007). The system usually consists of two sets of variables X and Y (as a concrete example, let us imagine for now X represents pixels of an image, and Y Boolean variables classifying the image). If the energy of the state, $E(X, Y)$, is low, then the classification is good. In many EBMs, the energy is similar to the Ising formula. In the well-known model of Boltzmann machine (Hinton et al., 1984) for example, if we ignore the distinction between the two set of variables and just refer to each variable as σ_i , the energy is equivalent to the Ising model:

$$E = - \sum_{i < j} W_{ij} \sigma_i \sigma_j - \sum_i \theta_i \sigma_i \quad (2)$$

When using Boltzmann machines for inference, the system is also similar to using an Ising machine, but with a difference in the meaning of the variables/spins. But by and large, Ising machines can accelerate inference of Boltzmann machines in a straightforward manner.

Training a Boltzmann machine is an entirely different matter. Unlike in an optimization problem where the weights are inputs, in training the weights are the output. In other words, training is the inverse of a combinatoric optimization problem. Like in many machine learning algorithms, training is done by using a gradient descent approach to

lower the loss function while iterating over a set of training samples. While we will get into the details later, a key point to emphasize here is that the key challenge in such a gradient descent algorithm often involves terms that are computationally intractable, leading to the necessity of approximation algorithms. Here, a nature-based computing substrate allows us to adopt approaches convenient or efficient for that substrate without the need to follow exactly the prevailing von Neumann algorithms.

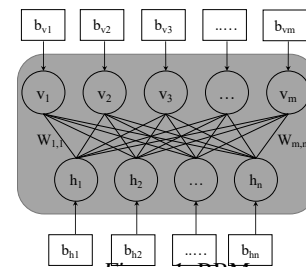
In this paper, we will show how a physical Ising machine can help accelerate an EBM both in training and in inference in a number of different ways. For this purpose, we choose a special case of Boltzmann machines called the Restricted Boltzmann Machine (RBM) as it is a widely-used algorithm that is heavily optimized for von Neumann architectures. RBMs (and its multi-layer variants) have found applications in specialized learning (Salakhutdinov & Hinton, 2009; Dahl et al., 2010; Hjelm et al., 2014; Wang et al., 2014; Ding et al., 2016; Zhang et al., 2016; Abdel-Zaher & Eldeib, 2016; Al-Waisy et al., 2021) and unsupervised learning (Salakhutdinov et al., 2007; Larochelle et al., 2009; Erhan et al., 2010; Hinton & Salakhutdinov, 2011; Fiore et al., 2013; Srivastava et al., 2013; Gouveia & Correia, 2017; Xie et al., 2018; Hernandez & Abad, 2018; Fatemi & Safayani, 2019; Wang et al., 2020).

An RBM has only connections between a visible node and a hidden node and no connections between two visible nodes or two hidden nodes as shown in Figure 1. As a result, the energy function is as follow:

$$E(v, h) = - \sum_i^m \sum_j^n v_i W_{ij} h_j - \sum_i b_{v_i} v_i - \sum_j b_{h_j} h_j \quad (3)$$

where $W_{i,j}$ is the coupling weight between visible unit v_i and hidden unit h_j ; and b_{v_i} and b_{h_j} are the biases for the corresponding visible and hidden units.

Similar to other neural networks, RBMs can be stacked into a multi-layer configuration to form a deep network. Specifically, two common variants are Deep Belief Networks (DBN) and Deep Boltzmann Machines



(DBM) (Salakhutdinov & Hinton, 2009; Hua et al., 2015). There are subtle differences between these variants and the simpler RBM. For the sake of clarity, we will focus on discussing RBM and follow conventional approaches when stacking multiple layers together. In other words, DBN/DBM-specific optimizations are outside the scope of this paper.

3 ARCHITECTURE

In this section, we discuss the architecture design issues. We start with our Ising machine substrate that will be the foundation for additional architecture support (Sec. 3.1). Next, we discuss a design where our modified Ising machine serves to provide acceleration for key computation in an otherwise conventional approach to the training of RBMs (Sec. 3.2). Finally we show that if we start from first principles, we can take a somewhat different approach than conventional training algorithm and leverage the strength of our Ising substrate as a practical Boltzmann sampler (Sec 3.3). The result is more flexibility in system design that ultimately leads to a more efficient design.

3.1 Ising machine substrate

As we discussed earlier, a number of physical substrates can leverage nature to perform optimization of an Ising formula. In principle, any such substrate can be used for our purpose of accelerating a machine learning algorithm. In practice, we aim for an integrated electronic design. This makes the BRIM design (Afoakwa et al., 2021) a much more convenient baseline to use. Figure 2 shows a high-level diagram of its architecture.

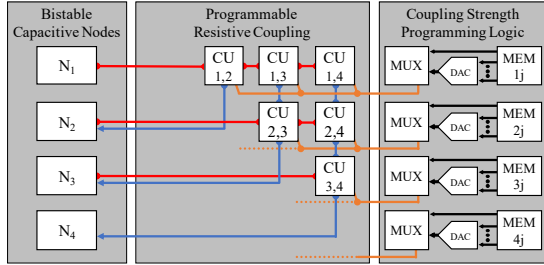


Figure 2. High-level BRIM showing bistable capacitive nodes with programmable resistive coupling, and its programming logic. Note that between every pair of nodes (say, N_1 and N_2), we only show one bi-directional coupling units ($CU_{1,2}$), resulting in an upper triangular coupling network. In an equivalent implementation, the coupling unit may consist of two uni-directional parts, forming a symmetric layout.

In this machine, each node consists of a capacitor and a feedback unit to make the capacitor bistable (1 or -1). A mesh of all-to-all programmable resistors serve to express the Ising formula the system is trying to optimize. When treated as a dynamic system, a Lyapunov analysis can be applied to the differential equations governing the nodal voltages. It can be shown that local minima of the Ising energy landscape are all stable states of the system (Afoakwa et al., 2021). Put more simply, starting from a given initial condition, this system of coupled nodes will seek a local minimum without explicit guidance from a controller. Extra annealing control is needed to inject random “spin flips” to escape a local minimum. This is analogous to accepting

a state of worse energy with non-zero probability in simulated annealing (Kirkpatrick et al., 1983).

In an RBM, the nodes are separated into a bipartite graph. For such a special graph, the architecture for our Ising machine substrate can be slightly modified to have nodes on two edges of the coupling network. In this structure, a visible node (v_i) can only be coupled to a hidden node (h_j) as shown in Figure 3. This layout significantly improves space efficiency compared to one that allows connection between all nodes. As a concrete example, one of our benchmarks uses 784 visible nodes and 200 hidden nodes. Mapping them on a generic all-to-all Ising substrate would need about 6 times more coupling units ($(784 + 200)^2$ vs 784×200).

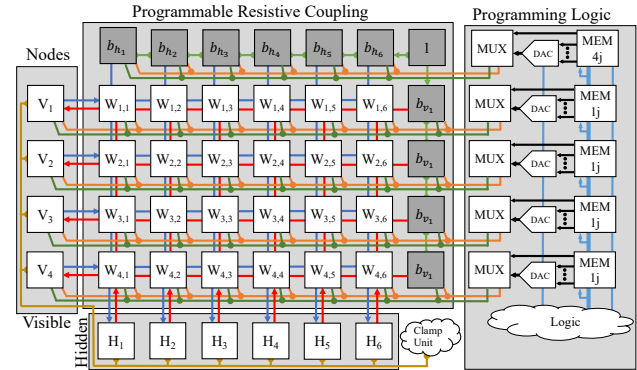


Figure 3. High-level RBM showing visible and hidden nodes, with clamping units to drive node biases, coupling mesh, and programming logic.

Finally, the nodes of the Ising machine can be augmented in the following ways to support operation of the RBM algorithm. In both training and inference, it is common to clamp the visible nodes or the hidden nodes to certain value. This can be easily achieved with a buffer connected to the nodal capacitor. One important detail is that the inputs to the visible nodes are usually multi-bit values and thus requires digital-to-analog conversion. Note that in the baseline Ising machine, the vast majority of the area is devoted to the coupling units as it scales with N^2 (N being the number nodes). Thus most addition to the node structure has a small impact to the system’s complexity and chip area.

3.2 Gibbs sampler architecture

We first discuss a variant of RBM accelerator that is more traditional: we are simply leveraging the Ising substrate to accelerate a portion of the software algorithm that naturally suits the hardware. For convenience, we name the accelerator design *Gibbs sampler* (GS) as it follows (a variant of) the traditional Gibbs sampling-based algorithm (Gelfand, 2000), which we show as Algorithm 1.

The algorithm: Here we see that in the training loop (lines 8 to 16), there are repeated calculations of $\langle v_{pos}^\top, h_{pos} \rangle$ and $\langle v_{neg}^\top, h_{neg} \rangle$. In a nutshell, the algorithm is a stochastic gradient descent and the training loop is calculating the stochastic gradient for every weight W_{ij} . In the so-called positive phase (lines 9, 10), a training sample v_{pos} is clamped to the visible nodes; and a corresponding sample for the hidden nodes h_{pos} is generated based on the conditional probability formula:

$$P(h_j = 1|v) = \sigma(b_{h_j} + \sum_i W_{ij}v_i) \quad (4)$$

where $\sigma(x)$ is the logistic function $1/(1 + e^{-x})$.

In the negative phase (lines 13, 14), a k -step Gibbs sampling is performed. Keeping the current hidden node values, we probabilistically generate a set of new visible nodes, with probabilities as follows.

$$P(v_i = 1|h) = \sigma(b_{v_i} + \sum_j W_{ij}h_j) \quad (5)$$

From there, the updated visible nodes project back to generate updated hidden nodes, forming one complete step of the Markov Chain Monte Carlo (MCMC) algorithm. In principle, one such step in the MCMC algorithm would make a rather poor sampling. In practice, a small number of k steps (a typical choice is 5) are chosen to balance the cost and the quality of the sampling. Such a k -step contrastive divergence algorithm is often referred to as CD- k .

Algorithm 1 Contrastive divergence algorithm for training

Input: training_data, learning_rate (α), CD_k , batch_size (bs)

Output: weights (W), visible bias (b_v), hidden bias (b_h)

```

1:  $W \leftarrow \text{random}(M \times N)$ 
2:  $b_v \leftarrow \text{zeros}(1 \times M)$ 
3:  $b_h \leftarrow \text{zeros}(1 \times N)$ 
4:  $\text{number of batches} = \frac{\text{size of training data}}{\text{batch.size}}$ 
5:
6: for  $s = 1, 2, \dots, \text{steps}$  do
7:   for  $b = 1, 2, \dots, \text{number of batches}$  do
8:     for  $i = 1, 2, \dots, bs$  do
9:        $v_{pos}[i] \leftarrow \text{training\_data}[(b-1) * bs + i]$ 
10:       $h_{pos}[i] \leftarrow \text{rand}() < \sigma((v_{pos}[i] \times W) + b_h)$ 
11:       $h_{neg}[i] \leftarrow h_{pos}[i]$ 
12:      for  $k = 1, 2, \dots, CD_k$  do
13:         $v_{neg}[i] \leftarrow \text{rand}() < \sigma((h_{neg}[i] \times W^\top) + b_v)$ 
14:         $h_{neg}[i] \leftarrow \text{rand}() < \sigma((v_{neg}[i] \times W) + b_h)$ 
15:      end for
16:    end for
17:     $W \leftarrow W + \alpha * (\langle v_{pos}^\top, h_{pos} \rangle - \langle v_{neg}^\top, h_{neg} \rangle)$ 
18:     $b_v \leftarrow b_v + \alpha * (v_{pos} - v_{neg})$ 
19:     $b_h \leftarrow b_h + \alpha * (h_{pos} - h_{neg})$ 
20:  end for
21: end for

```

Architectural support: At every learning step, the current weight matrix $[W_{ij}]_{M \times N}$ will be programmed to the

coupling array such that the resistance at each unit R_{ij} is proportional to $\frac{1}{W_{ij}}$. This step is just like programming the optimization formula in a standalone Ising machine. If we further clamp one set of nodes (say, visible) to fixed values, each coupling unit will produce a current equal to the voltage of the visible node divided by the resistance of the programmable coupling unit, which is equivalent to multiplying the corresponding weight in the matrix. Each hidden node, therefore, sees the sum of the current in the entire column. Used this way, the coupling array is effectively producing a vector-matrix multiplication operation.

At this stage, rather than reading out the resulting currents, we opt to feed the current through a non-linear circuit that produces the effect of the logistic function. In fact, when properly configured, a simple inverter can approximate the function admirably. Finally, the output of the logistic function is the probability of node being 1. This can also be supported with a relatively straightforward circuit: a comparator with the other input being fed with pseudo random voltage level. Details of circuit design and issues can be found in Appendix B.

Operation: With the architectural support described, much of the training loop in Algorithm 1 will be offloaded to the hardware. The remaining operations will be carried out on digital functional units such as a TPU. The overall operation sequence is as follows:

1. Initialization on TPU;
2. Programming the (initially random) coupling matrix and biases to the Ising substrate.
3. Clamping the visible units to a training sample (v_{pos});
4. Read out the hidden units (h_{pos}) after the Ising substrate finishes operation;
5. Perform k steps of Gibbs sampling by alternately clamping the hidden units and the visible units to produce samples on the other side.
6. Read out the final value from the visible (v_{neg}) and hidden units (h_{neg}).
7. Repeat steps 3 to 6 to collect the samples for calculating gradient descent.
8. Compute (on TPU) the new coupling matrix and biases by calculating gradient using the samples collected according to the following formula $(\langle v_{pos} h_{pos} \rangle - \langle v_{neg} h_{neg} \rangle)$.
9. Repeat from step 2 for subsequent minibatches.

3.3 Boltzmann gradient follower architecture

The system described in Sec. 3.2 represent an improvement over digital units as we shall see later. But this is largely due to the efficiency gain from approximate analog implementations. The benefit of nature-based computing is often much greater when we avoid frequent interactions between

specialized hardware and a more general-purpose computing substrate. For this to happen, we need to have a deeper understanding of the *intention* of the algorithm.

The goal of the MCMC algorithm: With RBM, the goal is to capture the training data with a probability distribution model. The probability is exponentially related to the energy of a state as in Boltzmann distribution (hence the name):

$$P(v, h) \propto e^{-E(v, h)} \quad (6)$$

Clearly the probabilities need to sum up to one, thus the equation for the probability of a particular state (v, h) is:

$$P(v, h) = \frac{1}{Z} e^{-E(v, h)}; \quad Z = \sum_{v, h} e^{-E(v, h)} \quad (7)$$

When we say the machine captures the training data, we mean the machine's model (weights and biases) maximizes the probability of all T training samples. In other words, it maximizes $\prod_{t=1}^m P(v^{(t)})$ where $v^{(t)}$ is the t^{th} training sample, or equivalently the sum of the log probability: $\sum_{t=1}^m \log(P(v^{(t)}))$. Note that $P(v) = \sum_h P(v, h)$. Since the probability is a function of the parameters (coupling weights and biases), we follow the gradient of each parameter. For the coupling parameter, the gradient is as follows:

$$\frac{\partial \sum_{t=1}^T \log P(v^{(t)})}{\partial W_{ij}} = \sum_{t=1}^T \frac{\partial [\log(\sum_h e^{-E(v^{(t)}, h)}) - \log(Z)]}{\partial W_{ij}} \quad (8)$$

For notional clarity, we now look only at the contribution of one training sample ($u = v^{(t)}$) to the gradient and focus on the first part in the numerator:

$$\begin{aligned} \frac{\partial \log(\sum_h e^{-E(u, h)})}{\partial W_{ij}} &= \frac{1}{\sum_h e^{-E(u, h)}} \frac{\partial \sum_h e^{-E(u, h)}}{\partial W_{ij}} \\ &= \frac{1}{\sum_h e^{-E(u, h)}} \sum_h e^{-E(u, h)} \frac{\partial(-E(u, h))}{\partial W_{ij}} \\ &= \frac{\sum_h e^{-E(u, h)} u_i h_j}{\sum_h e^{-E(u, h)}} = \langle u_i h_j \rangle_{data} \end{aligned} \quad (9)$$

Here the notation $\langle \cdot \rangle_{data}$ means the expectation with respect to the data, *i.e.*, keeping the data constant (u) and averaging over all possible h .

If we follow the same steps, the second part of the gradient ($\frac{\partial \log(Z)}{\partial W_{ij}}$) gives us:

$$\frac{\partial \log(Z)}{\partial W_{ij}} = \frac{\sum_{v, h} e^{-E(v, h)} v_i h_j}{\sum_{v, h} e^{-E(v, h)}} = \langle v_i h_j \rangle_{model} \quad (10)$$

Here the notation $\langle \cdot \rangle_{model}$ means the expectation with respect to the entire state space given by the current model (coupling parameters and biases).

As we can see, to calculate *any* parameter's gradient, we need to calculate the expectation of a large number of states, which is impractical. The common solution is an MCMC algorithm (*e.g.*, CD- k), just like simulated annealing in solving an Ising formulation problem. Both algorithms are inspired by Boltzmann statistics. The Ising machine substrate that we use *directly embodies* such statistics and can thus perform sampling of the state space with extraordinary efficiency. To see the efficiency, let us look at a concrete example. For a 784×200 RBM, the k -iteration software Gibbs sampling (lines 12 to 15 in Algorithm 1) is achieved by taking $s = k * (784 + 200)$ steps on the Markov chain and takes roughly $k \times 10^6$ instructions. This is equivalent to going through a trajectory on our dynamical system with roughly s phase points.

Architectural support: When we initialize the Ising substrate to some initial condition, it will proceed to traverse through the energy landscape directed by both the system's governing differential equations and the annealing control. This has the effect of "sampling" the state space and arguably produces samples better than the algorithmic random walk in CD- k . However, there is a problem: the production of the samples is much faster than the host computer can access and postprocess them to obtain the expectations. We propose, therefore, a more direct approach, where the sampled expectations ($\langle v_i h_j \rangle_{data}$ or $\langle v_i h_j \rangle_{model}$) are directly added to or subtracted from the model parameter (*e.g.*, W_{ij}) inside the Ising substrate, without involving the host.

In the CD- k algorithm, the accumulation is expressed as follows, where $\langle \cdot \rangle_s$ indicates the expectation over a set of samples s :

$$W_{ij}^{t+1} = W_{ij}^t + \alpha \left(\langle v_{pos} h_{pos} \rangle_s - \langle v_{neg} h_{neg} \rangle_s \right) \quad (11)$$

Here the expectations are accumulated over a minibatch of (say, $n = 500$) samples before being used to update the parameter to the next value. The choice of n is usually a matter of convenience for the software. For our hardware implementation convenience, our minibatch size is essentially one: Any increment or decrement takes effect directly on W_{ij} . Additionally, the circuit implementation adds an effective noise on top of the algorithmic noise due to stochastic sampling of the gradient. All non-idealities are faithfully modeled when we evaluate the system.

A fine point can be made here as to whether our learning algorithm produces a biased estimator or not. Our empirical analysis shows estimation bias appears to have no effect

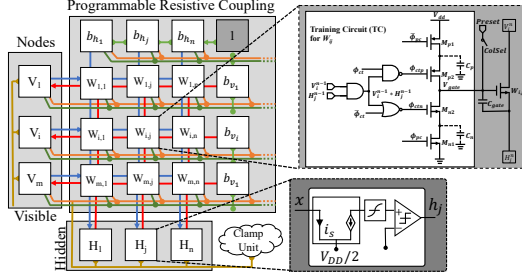


Figure 4. An architecture diagram of Boltzmann gradient follower.

on the ultimate accuracy measures. If anything, our modifications seem to reduce bias from the commonly used algorithms as detailed in Appendix A.

For negative phase samples, we use p different initial conditions for the hidden units ($h^{(m)}, m = 1..p$) to allow p independent random walks. These are often referred to as p particles. After each positive phase, we load one of the particles (say, $h^{(3)}$); perform annealing of the Ising machine (equivalent to the random walk of the von Neumann algorithm); take a sample of $v_{neg}h_{neg}$; and store the resulting hidden unit values back to $h^{(3)}$.

The parameters are physically expressed by the conductance of configurable resistors. The resistors are implemented by transistors with variable gate-source voltages. Increasing and decreasing the parameters can be achieved by raising or lowering the gate voltage. This in turn is done by a charge-redistribution circuit detailed in Appendix B.

Finally, since the entire learning is now conducted inside the (augmented) Ising substrate, the coupling unit is larger (Fig. 4). Furthermore, the trained results need to be read out at the end of the learning process, this requires extra analog-to-digital converters (ADC) which are expensive converters. Nevertheless, keep in mind that they are only used once at the end of the entire algorithm.

In short, though the architecture needs some non-trivial new circuits and small modifications to the operating algorithm, it carries out the *intention* of a traditional software implementation. As we will see, the resulting quality is no different from a software implementation even under non-trivial noise considerations.

Operation: Figure 4 shows the proposed Boltzmann gradient follower architecture. The key addition is to the coupling unit where the programmable resistor serving as the weight can be adjusted in place. With this architecture, the digital (host) computer takes a much more peripheral role, mostly setting the system up, feeding data at a fixed frequency, and finally reading the results. The operation can be described as follows:

1. Initialize the weights and biases.⁴
2. The host would send training samples to latches at the visible units.
3. The machine will clamp the data, wait for a predetermined time for the hidden units to settle. The resulting sample (v_{pos}, h_{pos}) will increment W_{ij} .
4. The machine will then load one of p particles and start annealing process.
5. After annealing, the resulting sample (v_{neg}, h_{neg}) will decrement W_{ij} .
6. The process (2-5) is repeated for a programmable number of learning steps. Then the ADCs will read out the coupling voltages one column at a time.

4 EXPERIMENTAL ANALYSIS

To better understand the characteristics of our augmented Ising substrate for EBMs, we compare various metrics between our proposed design and TPU (Jouppi et al., 2017). It is worth noting up front that an evolutionary perspective is needed when viewing the results. Both digital numerical architectures and nature-based computing systems will evolve. Design refinement can bring significant changes to these metrics. More importantly, the line between the two groups will continue to blur and cross pollination is very much an intended consequence.

We next describe the experimental setup including benchmark RBMs and DBN models; then show quantitative comparisons between a TPU and a noiseless model of our analog design in terms of energy efficiency and throughput; and finally present a few in-depth analyses to help understand the how the system behaves.

4.1 Experimental Setup

Datasets and metric: To evaluate the systems discussed, we trained them on different applications like image classification, recommendation systems and anomaly detection. For image classifications we use many datasets including handwritten digits (MNIST) (Deng, 2012), Japanese letters (KMNIST) (Clanuwat et al., 2018), fashion images (FMNIST) (Xiao et al., 2017), extended handwritten alphabet images (EMNIST) (Cohen et al., 2017), toy dataset (SmallNorb) (LeCun et al., 2004), medium color images (CIFAR10) (Krizhevsky, 2009), and larger images of 101 categories of objects (Caltech 101) (Li et al., 2022). Image sizes range from 28x28 gray scale (NIST), to 300x200 color image (Caltech). RBM and Deep Belief Network (DBN) are directly attached to the images in the NIST

⁴Note that for common practice, the weights are initialized to small random values. This could certainly be implemented by the hardware itself. But programmable initial conditions may be useful for special purposes in training (e.g., research) and certainly for inference.

datasets while Convolution RBM algorithm (Coates et al., 2011) is used for CIFAR10 and SmallNorb datasets, and transfer learning is used to train using Caltech101 dataset following (Zhao et al., 2017; Wang et al., 2019).⁵

To train RBM as a recommendation system (Verma et al., 2017) and anomaly detector (Pumsirirat & Yan, 2018) we use 100k MovieLens dataset (Harper & Konstan, 2015) and “European Credit Card Fraud Detection” (Dal Pozzolo et al., 2017) dataset respectively. The learning rate used to train these models is 0.1 and size of RBM and DBN configurations are shown in Table 1. Since RBMs are unsupervised models, one way to quantify the quality of training is the average log probability of the training samples which can be measured using annealed importance sampling (Salakhutdinov & Murray, 2008). We also report some common metrics like classification accuracy using logistic regression layer at the end for image classification, mean absolute error (MAE) of test data and projected data for recommendation systems and area under Receiver operating characteristic (ROC) curve for Anomaly detection.

Table 1. Dataset parameters of different types of Neural Networks used in evaluation.

Datasets	RBM	DBN-DNN (Hinton et al., 2012)
MNIST	784-200	784-500-500-10
KMNIST	784-500	784-500-1000-10
FMNIST	784-784	784-784-1000-10
EMNIST	784-1024	784-784-784-26
CIFAR10	108-1024	-
SmallNorb	36-1024	-
Caltech101	-	9216-5000-10000
Recommendation systems	943-100	-
Anomaly detection	28-10	-

Modeling: Behavioral models of Gibbs sampler (GS) and Boltzmann gradient follower (BGF) were developed using Matlab. All circuits are modeled in Cadence 45nm using Generic Process Design Kit (GPDK045) to obtain power and area. We designed a 32x32 node Boltzmann gradient follower in cadence to test the behavioral models. We used these behavioral models to obtain performance and noise analysis. We assume the system has enough nodes to fit the largest problems in the set. Thus execution time is just the product of the number of iterations and the cycle count per iteration. Anything not carried out on our hardware is done on the host machine, which we take to be the same TPU as the baseline. The area and power consumed by the TPU unit were obtained from (Jouppi et al., 2017), which uses a 28nm technology. We used 8-bit precision ADCs to read out the final trained weights. To input training data, we used 8-bit precision DTCs. We adopt DTCs, and ADCs based on the measurement-validated designs in the follow-

⁵We use convolution parameters of Alexnet (Krizhevsky et al., 2012) pretrained on Imagenet dataset (Deng et al., 2009) for our convolution layers. We have a softmax layer at the end.

ing papers (Li et al., 2017), (Kull et al., 2013), respectively.

4.2 Execution Speed

We first consider the execution speed of the two proposed architectures: the Gibbs sampler (GS) and the Boltzmann gradient follower (BGF). The operating frequency is 1GHZ for both. For comparison, we use TPU (v1) as a baseline.

Fig. 5 shows normalized execution time of different benchmarks. As we can see, for the bigger networks, a bigger portion of our hardware is being utilized and the speed advantage will increase. Here we assume every benchmark fits on the hardware. Most datasets that we have comfortably fit inside a small die.

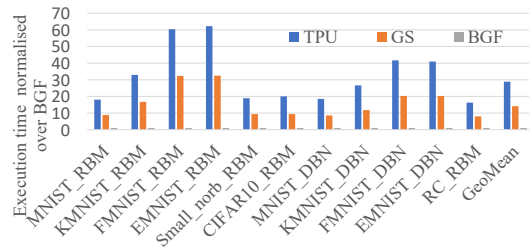


Figure 5. Execution time normalized to that of BGF for different RBMs and image batch size of 500.

Overall, in a first-order approximation, adding a GS or a BGF to a TPU array will increase area fractionally (more on that later) but improve speed by a geometric mean of 2x (GS) or 29x (BGF). Note that here we do not include Caltech101 benchmark which uses a much larger network with a correspondingly larger speedup of 6000x. At the same time, the chip area of BGF will need to grow to about $226mm^2$

4.3 Energy Consumption

A primary source of fundamental efficiency of an Ising substrate comes from the fact that many algorithms are *mimicking* nature, whereas our hardware directly embodies that nature. For instance, in a typical step of MCMC, flipping one node requires roughly $O(N)$ multiply-accumulate (MAC) operations followed by some probability sampling. Ignoring the probability sampling, which may be much more costly, just a MAC operation costs on the order of a pJ. For the problems discussed, $N \approx 1000$. So one such flip requires the order of nJ using conventional digital computation. In contrast, in BRIM, flipping a node involves a distributed network of currents charging/discharging a nodal capacitor. With nodal capacitors on the order of 50 fF and a voltage of roughly 1V, flipping of a node takes on the order of 100 fJ. Thus, an Ising substrate has the potential to be about 4 orders of magnitude more efficient compared to a conventional computational substrate.

Regarding the entire system, the energy savings will depend on many factors not included in the simplified analysis above. With the technology difference in mind, we can compare the energy consumption of different benchmarks shown in Figure 6. All energy results are normalized to that of the Boltzmann gradient follower.

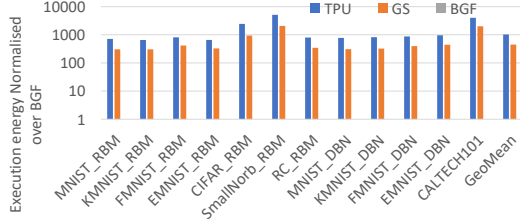


Figure 6. Energy consumption of TPU and GS over various benchmarks normalized over BGF for image batch size of 500.

Our accelerators are more energy efficient in the effective operations they carry out than digital TPU operations prescribed by the algorithm. Overall, we see improvements of around 1000x for BGF. Two qualitative points are worth mentioning. On the one hand, digital circuit can still improve and more efficient designs can further reduce per-operation cost. On the other hand, the type of short random walks performed on our Boltzmann gradient follower architecture are not the most efficient use of the architecture. Further algorithm innovation may well find applications that fully utilize the ability of ours and similar nature-based systems.

Table 2. Area and power of sub-units of Gibbs sampler and Boltzmann gradient follower at different number of nodes(N). CU = Coupling unit; SU = Sigmoid unit; RNG = Random number Generator; DTC= Digital to Time Converter

Components / Nodes	400 × 400		800 × 800		1600 × 1600	
	area (mm ²)	power (mW)	area (mm ²)	power (mW)	area (mm ²)	power (mW)
CU (Gibbs) (N^2)	0.24	56	0.96	101	3.84	192
CU (BGF) (N^2)	0.36	96	1.45	262	5.76	834
SU (N)	0.002	0.97	0.004	1.94	0.008	4
Comparator (N)	0.03	2	0.06	4	0.12	8
DTC (N)	0.1	5	0.19	10	0.39	20
RNG (N)	0.006	12	0.012	24	0.03	48
Total(Gibbs)	0.38	78	1.23	148	4.38	295
Total(BGF)	0.5	116	1.71	301	6.3	910

Finally, we look at the chip area estimates. Again, with the technology difference this is also not a direct comparison. Nevertheless, our baseline 28nm TPU takes about 330mm² with 24% of it being the MAC array. In comparison, the area and power of BGF and its building blocks are shown in Table 2. Because the coupling unit is by far the most numerous elements (roughly $O(N^2)$ vs $O(N)$ for other units), the area is largely determined by the coupling units. Assuming a 1600 × 1600 array, a Boltzmann gradi-

ent follower costs about 6.3mm² which is rather negligible when compared to TPU area. As shown in Table 3, BGF are much more efficient – in this specialized algorithm – than TPU or the state-of-the-art computational accelerators.

Table 3. Comparison between different accelerators.

Accelerators	TOPs/s × mm ²	TOPs/W
TPU (Jouppi et al., 2017)	1.16	9.56
TIMELY (Li et al., 2020)	38.33	21.00
BGF(1600 × 1600)	812	5600

4.4 Impact of algorithmic change

From a first-principle analysis, our Boltzmann gradient follower architecture simply implements a different style of stochastic gradient descent. It will not give us the exact same trained weights, but should provide similar solution quality to the end user. We now analyze numerically the change resulted from the algorithmic change. We use two metrics as discussed before: the average log probability of the training samples and classification accuracy. Fig. 7 shows the average log probability of models obtained using different methods (CD-1, CD-10 and our modified versions to Boltzmann gradient follower) over a period of training with different data sets. Note that the log probability is computationally intractable and thus approximated with AIS (Salakhutdinov & Murray, 2008) as already mentioned in Sec. 3.3. The result should therefore not be read with too much precision. Indeed, in some data sets (*e.g.*, CIFAR10), the same AIS mechanism fails altogether to produce a finite estimate on the partition function. We show a few example data sets.

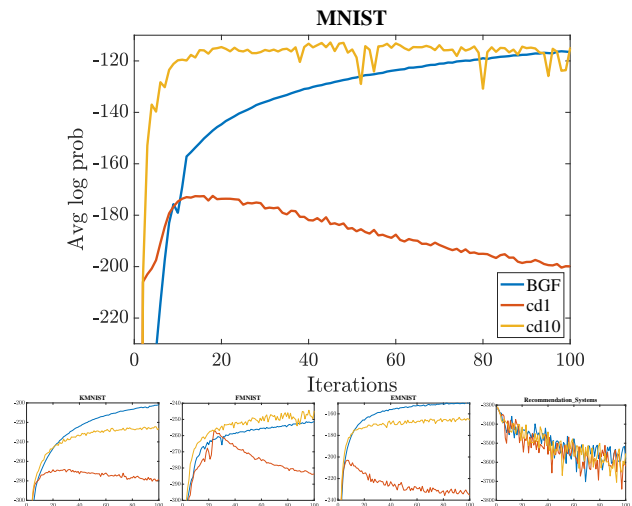


Figure 7. Average log probability of different models (higher is better) of conventional algorithms (CD-1 and CD-10) and our modified algorithm used for Boltzmann gradient follower (BGF). The same legend applies to the thumbnails too.

As we can see, in general, trajectories of log probability increase over time, and often quite substantially. This means the trained models approximate the probability distribution of training data better over time. The exact trajectory, however, is highly variable even under common practices of CD- k with different k values. Our modified algorithm is understandably producing its own trajectory. Compared to CD-10, the difference in trajectory is often less pronounced than that resulting from choosing a small k for expediency. In addition to the uncertainty in the log probability estimate itself and keep in mind that beyond a certain point, one could argue that better log probability is simply a result of overfitting. Thus we also show classification errors in Table 4. We see that in benchmarks where rounding is applied by the tool, there is no observable difference between common practice and our algorithm. In the benchmark with a bit more reported precision, we can see the difference is negligible.

Table 4. Test accuracy obtained by different types of Neural Network Models for each data set USING different algorithm. The accuracy is rounded by "sklearn" (python library) function.

Datasets	RBM cd-10	DBN-DDN cd-10	RBM BGF	DBN-DDN BGF
MNIST	97%	99%	97%	99%
KMNIST	88%	93%	88%	93%
FMNIST	87%	90%	87%	90%
EMNIST	89%	95%	89%	95%
CIFAR10	73%	-	73%	-
SmallNORB	84%	-	84%	-
Caltech101	-	89%	-	89%
RC system MAE	0.7642	-	0.7646	-
Anomaly detection AUC	0.96	-	0.96	-

Overall, the main takeaway point is this: We made small modifications to the common practice algorithm for the convenience of implementation. From a first principle perspective, this is no different than choosing CD- k over, say, the impractical maximum likelihood learning, or choosing a random k value in CD- k for expediency alone. Empirical observations now suggest that these changes indeed do not affect the efficacy of the learning approach.

4.5 Impact of noise on training

Finally, we look at the impact of noise and variation on solution quality. Until this point, the results are assuming the analog hardware suffers from no noise or variation. To simulate process variations and circuit noise, we inject both static variation on the resistance of the coupling units and dynamic noises at both nodes and coupling units. The noise and variation are generated by Gaussian distribution with root mean square (RMS) values between 3% and 30%. Different results are thus characterized by a pair $(RMS_{variation}, RMS_{noise})$. In Figure 8 we show the same smoothed result of average log probability for 25

combinations.

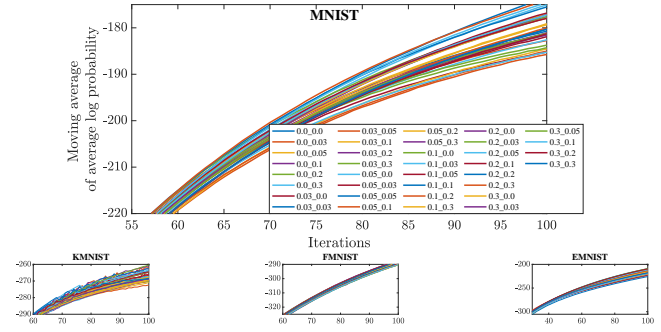


Figure 8. Moving average of mean log probability of different models under varying amount of injected noise and variations. The data are smoothed using a moving average of 10 points.

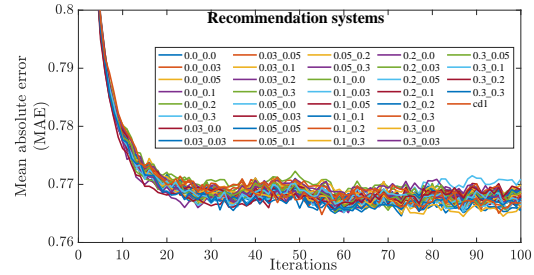


Figure 9. Mean absolute error (MAE) of different models under varying amount of injected noise and variations. Final MAE ranges between 0.771 and 0.765.

In general, the message is perhaps somewhat predictable: When the combination of noise and variation is not too extreme (e.g., $< 10\%$ each), the impact on log probability is negligible. In many cases, the loss is smaller than that gained by modifying the algorithm to suit our Boltzmann gradient follower. But even for the more extreme variation and noise configurations the impact on log probability does not appear significant. And the final inference accuracy is unchanged for all image-based benchmarks. For Recommendation system and anomaly detection benchmarks, the final results do show a little variation as shown in Fig. 9 and 10.

To sum, while the analog circuits are subject to noise, they can competently perform the gradient descent function under even significant amount of noise without affecting the quality of the overall training process.

4.6 Discussions

Overall, experimental analysis of the two architectures provides some evidence that even without new algorithms specifically exploiting the capability of the hardware, we can obtain substantial performance and energy benefits

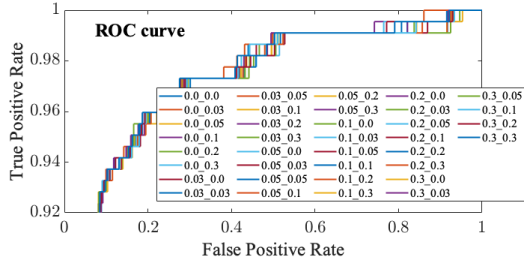


Figure 10. Roc curves of different models under varying amount of injected noise and variations. Final AUC ranges between 0.964 and 0.967.

with a very small additional chip footprint. On the other hand, computational substrates such as TPU are clearly much more general-purpose. At this stage, our analysis does not yet suggest that they are compelling designs per se. But we believe it shows that there is potential in the general direction for a number of reasons:

1. Ising substrates are already quite useful in accelerating a broad class of optimization problems. They could become even more versatile and widely used in the future. Thus the incremental cost of additional architectural support will become lower still.
2. Our designs are but an initial exploration. Further research could improve system’s versatility and performance by, for example, reconfigurability and support for exploiting training set parallelism.
3. Energy-based models have many good qualities but are notoriously expensive to train. With the advent of prototype Ising machines and systems such as Boltzmann gradient follower, better algorithms may follow.

5 CONCLUSIONS

Statistical physics has inspired a lot of effective algorithms. Physical Ising machines are dynamical systems that embody the physics underlying popular algorithms such as simulated annealing, RBM, and other derivative algorithms. As a result, an Ising machine substrate (when done right) can be used as extreme accelerators for certain part of these physics-inspired algorithms. In this paper, we showcased two different designs that augment an Ising substrate with extra circuit to support RBM training. We show that with some small changes, an Ising machine can easily serve as a Gibbs sampler to accelerate the RBM algorithm. With more substantial changes, the substrate can serve as a Boltzmann sampler while following the gradient to train RBM without any additional host computation. Compared to an idealized TPU host significantly larger in chip area, such a Boltzmann gradient follower can achieve some 29x speedup and 1000x energy savings – though these systems are far less general-purpose than TPUs. With further re-

search, we believe that the hardware software co-designed nature-based computing systems can be an important new architectural modality.

A BIAS OF LEARNING ALGORITHMS

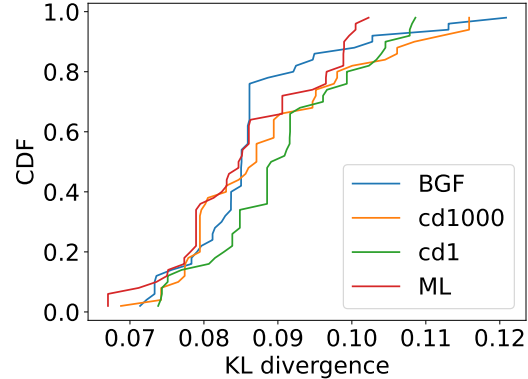


Figure 11. Cumulative probability distribution of KL divergence of CD and BGF training result against ground truth. In other words, every point (x, y) on the curve shows $y\%$ of training distribution have a final KL divergence of x or less from the ground truth.

Unlike a maximum likelihood (ML) learning algorithm the contrastive divergence (CD) algorithm is known to be biased. This means that the fixed points of the CD algorithm is not the same as that of the ML algorithm. Although the topic generated numerous publications, in practical terms the issue is insignificant. First, the bias is shown to be small. Second, the ultimate goal of the algorithm is to capture the training data well enough to be useful. Nevertheless, we show empirical observations of the bias for our modified training algorithm. For this experiment, we use the same methodology Carreira-Perpinan and Hinton used in their original investigation (Carreira-Perpinan & Hinton, 2005).

We use a small enough system size that the ground truth can be obtained via enumeration. The system consists of 12 visible units and 4 hidden units, all binary. We generate 60 different distributions of 100 training images randomly. We then execute ML, CD, and our training algorithm (BGF) for the same 1000 iterations to obtain the weights. Finally, we compare the resulting probability distribution against the ground truth by measuring the KL divergence. Each run of the algorithm produces one KL divergence measure. We repeat 400 runs for each algorithm from different random initial conditions. The resulting 400 different measures are plotted as cumulative probability distribution shown in Fig.11.

We can see that all the algorithms have a fairly similar bias characteristic. This is not not surprising since BGF is really a modified CD algorithm. However, because of the inherent speed in exploring the phase space, BGF can be thought of

as CD- k with a very large k . As $k \rightarrow \infty$, CD- k effectively becomes ML. As a result, we see BGF indeed offers less chance of a larger KL divergence compared to conventional CD- k . Overall, the takeaway point is clear. Our BGF does not create a problem of biased estimation. If anything, it improves the bias characteristic of the commonly used von Neumann algorithm.

B CIRCUIT

In addition to the circuits needed to implement the baseline Ising substrate, we need extra circuits in the nodes to make them probabilistic according to RBM algorithms, which are summarized in Fig. 12. Specifically, we need a current summing circuit (Sec. B.1), a sigmoid function (Sec. B.2), and a random number generator (Sec. B.3). Finally, for the Boltzmann gradient follower architecture, the coupling unit is discussed in (Sec. B.4).

B.1 Current summation

The current summation depicted in Fig. 12(e) is performed in two non-overlapping clock phases (ϕ and $\bar{\phi}$). During the reset phase ($\bar{\phi}$), both the hidden node capacitor h_j and the column bus connecting visible nodes to the hidden node h_j are pre-charged to $V_{CM} = V_{dd}/2$. During the subsequent integration phase (ϕ), the capacitor h_j is connected to the column bus and integrates all the currents for a fixed time interval t_{int} producing an output voltage equal to $\frac{t_{int}}{C_{h_j}} \sum_i v_i / R_{i,j}$ which is then sent to a sigmoid unit.

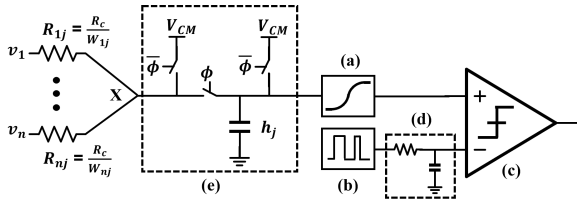


Figure 12. High-level block diagram of a node. Detailed implementations of (a), (b) and (c) are depicted in Fig. 13.

B.2 Sigmoid unit

In general, a sigmoid function is monotonic, and has a first derivative which is bell shaped. The simplest circuit which exhibits similar characteristics is an inverter, as shown in Fig. 13(a). A couple of issues need to be addressed before using an inverter as a sigmoid unit. First, the transfer function of a typical inverter used as a logic-gate consists of three distinct regions (i.e., two triode regions closer to the power rails and a steep region in the middle due to an inverter's high gain around the threshold), while a sigmoid function typically has a smoother transfer function. The inverter's transfer function is made more closely aligned with the sigmoid function by reducing its gain, which could be

achieved by increasing the transistors' channel lengths and adding a loading resistor at the output. The second issue is that the inverter's transfer function is a vertically flipped image of a general sigmoid function, which is mitigated by introducing an additional inversion in the subsequent stages (e.g., using an inverting comparator as shown in Fig. 13(c)).

B.3 Random number generator

Thermal noise from electronic devices can be utilized to generate randomness. The circuit shown in Fig. 13(b) is one kind of random number generator (RNG) and its operation is as follows. When ϕ is low, nodes A and B are pulled up to V_{dd} , which is a metastability point. When ϕ goes high, the circuit enters into the evaluation phase: both nodes discharge towards the switching point of the inverter, then the large gain at this point pulls one of the nodes to V_{dd} , while the other is pulled down to ground, depends on the sign of the differential thermal noise. The RNG circuit itself produces a binary random sequence (i.e., the output is either V_{dd} or 0), which is not directly suitable to achieve probabilistic sampling at the output of the sigmoid function. However, the binary random sequence at the output of the RNG is readily converted to a white-noise uniformly distributed from 0 to V_{dd} , by applying an RC low-pass filter as shown in Fig. 12(d). The resulting white-noise is then compared against the output of the sigmoid function in a standard dynamic comparator (Baker, 2019) (shown in Fig. 13(c)) to achieve probabilistic sampling.

B.4 Coupling unit for Boltzmann gradient follower

For each coupling unit representing a coupling parameter ($W_{i,j}$), a training circuit is added to allow the Boltzmann gradient follower algorithm to adjust $W_{i,j}$. This adjustment is achieved through a charge redistribution-based CMOS charge pump circuit shown in Fig. 14. The charge pump consists of two pre-charging transistors (M_{p1} and M_{n1}) and two charge transfer transistors (M_{p2} and M_{n2}), driven by two non-overlapping control signals (ϕ_{pc} and ϕ_{ct}). C_p and C_n are parasitic capacitances at those internal nodes. Both are controlled by ϕ_{ct} and $V_i^{n-1} * H_j^{n-1}$.

During the pre-charge phase (ϕ_{pc} is high), C_p will be precharged to V_{dd} , and hence the amount of charges stored on C_p is $C_p V_{dd}$. At the same time, C_n is discharged to ground. During the charge transfer phase (ϕ_{pc} is low), if $V_i^{n-1} * H_j^{n-1} = 1$, M_{p2} will be activated leading to charges redistributed from C_p to C_{gate} , and hence increase V_{gate} . If $V_i^{n-1} * H_j^{n-1} = 0$, M_{n2} will be activated to redistribute charges on C_{gate} with C_n , and hence V_{gate} decreases. $W_{i,j}$ is updated according to the increment or decrement of V_{gate} .

Due to the non-overlapping control signals, there will be no current path directly connecting C_{gate} to V_{dd} or ground. So

- Dal Pozzolo, A., Boracchi, G., Caelen, O., Alippi, C., and Bontempi, G. Credit card fraud detection: a realistic modeling and a novel learning strategy. *IEEE transactions on neural networks and learning systems*, 29(8): 3784–3797, 2017.
- Deng, J., Dong, W., Socher, R., Li, L.-J., Li, K., and Fei-Fei, L. Imagenet: A large-scale hierarchical image database. In *2009 IEEE conference on computer vision and pattern recognition*, pp. 248–255. Ieee, 2009.
- Deng, L. The mnist database of handwritten digit images for machine learning research [best of the web]. *IEEE Signal Processing Magazine*, 29(6):141–142, 2012.
- Ding, S., Zhang, J., Zhang, N., and Hou, Y. Boltzmann machine and its applications in image recognition. In Shi, Z., Vadera, S., and Li, G. (eds.), *Intelligent Information Processing VIII*, pp. 108–118, Cham, 2016. Springer International Publishing. ISBN 978-3-319-48390-0.
- Erhan, D., Courville, A., Bengio, Y., and Vincent, P. Why does unsupervised pre-training help deep learning? In *Proceedings of the thirteenth international conference on artificial intelligence and statistics*, pp. 201–208. JMLR Workshop and Conference Proceedings, 2010.
- Fatemi, M. and Safayani, M. Joint sentiment/topic modeling on text data using a boosted restricted boltzmann machine. *Multimedia Tools and Applications*, 78(15): 20637–20653, 2019.
- Fiore, U., Palmieri, F., Castiglione, A., and De Santis, A. Network anomaly detection with the restricted boltzmann machine. *Neurocomputing*, 122:13–23, 2013.
- Gelfand, A. E. Gibbs sampling. *Journal of the American statistical Association*, 95(452):1300–1304, 2000.
- Gouveia, A. and Correia, M. A systematic approach for the application of restricted boltzmann machines in network intrusion detection. In *International Work-Conference on Artificial Neural Networks*, pp. 432–446. Springer, 2017.
- Hamerly, R., Inagaki, T., McMahon, P. L., Venturelli, D., Marandi, A., Onodera, T., Ng, E., Langrock, C., Inaba, K., et al. Scaling advantages of all-to-all connectivity in physical annealers: the coherent ising machine vs. d-wave 2000q. *arXiv:arXiv:1807.00089*, 2018.
- Hamerly, R., Inagaki, T., McMahon, P. L., Venturelli, D., Marandi, A., Onodera, T., Ng, E., Langrock, C., Inaba, K., Honjo, T., et al. Experimental investigation of performance differences between coherent ising machines and a quantum annealer. *Science advances*, 5(5):eaau0823, 2019a.
- Hamerly, R., Sludds, A., Bernstein, L., Prabhu, M., Roques-Carmes, C., Carolan, J., Yamamoto, Y., Soljačić, M., and Englund, D. Towards large-scale photonic neural-network accelerators. In *2019 IEEE International Electron Devices Meeting (IEDM)*, pp. 22–8. IEEE, 2019b.
- Harper, F. M. and Konstan, J. A. The movielens datasets: History and context. *Acm transactions on interactive intelligent systems (tiis)*, 5(4):1–19, 2015.
- Hernandez, J. and Abad, A. G. Learning from multivariate discrete sequential data using a restricted boltzmann machine model. In *2018 IEEE 1st Colombian Conference on Applications in Computational Intelligence (ColCACI)*, pp. 1–6. IEEE, 2018.
- Hinton, G. The forward-forward algorithm: Some preliminary investigations. *arXiv preprint arXiv:2212.13345*, 2022.
- Hinton, G. and Salakhutdinov, R. Discovering binary codes for documents by learning deep generative models. *Topics in Cognitive Science*, 3(1):74–91, 2011.
- Hinton, G., Deng, L., Yu, D., Dahl, G. E., Mohamed, A.-r., Jaitly, N., Senior, A., Vanhoucke, V., Nguyen, P., Sainath, T. N., et al. Deep neural networks for acoustic modeling in speech recognition: The shared views of four research groups. *IEEE Signal processing magazine*, 29(6):82–97, 2012.
- Hinton, G. E., Sejnowski, T. J., and Ackley, D. H. *Boltzmann machines: Constraint satisfaction networks that learn*. Carnegie-Mellon University, Department of Computer Science Pittsburgh, PA, 1984.
- Hjelm, R. D., Calhoun, V. D., Salakhutdinov, R., Allen, E. A., Adali, T., and Plis, S. M. Restricted boltzmann machines for neuroimaging: An application in identifying intrinsic networks. *NeuroImage*, 96:245–260, 2014. ISSN 1053-8119. doi: <https://doi.org/10.1016/j.neuroimage.2014.03.048>.
- Hua, Y., Guo, J., and Zhao, H. Deep belief networks and deep learning. In *Proceedings of 2015 International Conference on Intelligent Computing and Internet of Things*, pp. 1–4. IEEE, 2015.
- Inagaki, T., Haribara, Y., Igarashi, K., Sonobe, T., Tamate, S., Honjo, T., Marandi, A., McMahon, P. L., Umeki, T., Enbutsu, K., et al. A coherent ising machine for 2000-node optimization problems. *Science*, 354(6312):603–606, 2016.
- Jouppi, N. P., Young, C., Patil, N., Patterson, D., Agrawal, G., Bajwa, R., Bates, S., Bhatia, S., Boden, N., Borchers, A., et al. In-datacenter performance analysis of a tensor processing unit. In *Proceedings of the 44th Annual International Symposium on Computer Architecture*, pp. 1–12, 2017.
- Karp, R. M. Reducibility among combinatorial problems. In *Complexity of computer computations*, pp. 85–103. Springer, 1972.

- Kim, K., Chang, M.-S., Korenblit, S., Islam, R., Edwards, E. E., Freericks, J. K., Lin, G.-D., Duan, L.-M., and Monroe, C. Quantum simulation of frustrated ising spins with trapped ions. *Nature*, 465(7298):590–593, 2010.
- King, A. D., Carrasquilla, J., Raymond, J., Ozfidan, I., Andriyash, E., Berkley, A., Reis, M., Lanting, T., Harris, R., Altomare, F., et al. Observation of topological phenomena in a programmable lattice of 1,800 qubits. *Nature*, 560(7719):456–460, 2018.
- Kirkpatrick, S., Gelatt, C. D., and Vecchi, M. P. Optimization by simulated annealing. *Science*, 220(4598):671–680, 1983. ISSN 0036-8075. doi: 10.1126/science.220.4598.671.
- Krizhevsky, A. Learning multiple layers of features from tiny images. Technical report, university of toronto, 2009.
- Krizhevsky, A., Sutskever, I., and Hinton, G. E. Imagenet classification with deep convolutional neural networks. *Advances in neural information processing systems*, 25, 2012.
- Kull, L., Toifl, T., Schmatz, M., Francese, P. A., Menolfi, C., Brändli, M., Kossel, M., Morf, T., Andersen, T. M., and Leblebici, Y. A 3.1 mw 8b 1.2 gs/s single-channel asynchronous sar adc with alternate comparators for enhanced speed in 32 nm digital soi cmos. *IEEE Journal of Solid-State Circuits*, 48(12):3049–3058, 2013. doi: 10.1109/JSSC.2013.2279571.
- Larochelle, H., Bengio, Y., Louradour, J., and Lamblin, P. Exploring strategies for training deep neural networks. *Journal of machine learning research*, 10(1), 2009.
- LeCun, Y., Huang, F. J., and Bottou, L. Learning methods for generic object recognition with invariance to pose and lighting. In *Proceedings of the 2004 IEEE Computer Society Conference on Computer Vision and Pattern Recognition, 2004. CVPR 2004.*, volume 2, pp. II–104. IEEE, 2004.
- LeCun, Y., Chopra, S., Ranzato, M., and Huang, F.-J. Energy-based models in document recognition and computer vision. In *Ninth International Conference on Document Analysis and Recognition (ICDAR 2007)*, volume 1, pp. 337–341. IEEE, 2007.
- Li, F.-F., Andreeto, M., Ranzato, M., and Perona, P. Caltech 101, 2022. URL <https://data.caltech.edu/records/20086>.
- Li, M.-R., Yang, C.-H., and Ueng, Y.-L. A 5.28-gb/s ldpc decoder with time-domain signal processing for ieee 802.15.3c applications. *IEEE Journal of Solid-State Circuits*, 52(2):592–604, 2017. doi: 10.1109/JSSC.2016.2624983.
- Li, W., Xu, P., Zhao, Y., Li, H., Xie, Y., and Lin, Y. Timely: Pushing data movements and interfaces in pim accelerators towards local and in time domain. In *2020 ACM/IEEE 47th Annual International Symposium on Computer Architecture (ISCA)*, pp. 832–845. IEEE, 2020.
- Liu, Z., Yang, Y., Pan, Z., Sharma, A., Hasan, A., Ding, C., Li, A., Huang, M., and Geng, T. Ising-cf: A pathbreaking collaborative filtering method through efficient ising machine learning. In *Proceedings of the 60th ACM/IEEE Design Automation Conference*, 2023.
- Lucas, A. Ising formulations of many np problems. *Frontiers in Physics*, 2:5, 2014.
- McMahon, P. L., Marandi, A., Haribara, Y., Hamerly, R., Langrock, C., Tamate, S., Inagaki, T., Takesue, H., Utsunomiya, S., Aihara, K., Byer, R. L., Fejer, M. M., Mabuchi, H., and Yamamoto, Y. A fully programmable 100-spin coherent ising machine with all-to-all connections. *Science*, 354(6312):614–617, 2016. doi: 10.1126/science.aah5178.
- Narayanan, A. and Moore, M. Quantum-inspired genetic algorithms. In *Proceedings of IEEE International Conference on Evolutionary Computation*, pp. 61–66, 1996. doi: 10.1109/ICEC.1996.542334.
- Pan, Z., Sharma, A., Hu, J. Y.-C., Liu, Z., Li, A., Liu, H., Huang, M., and Geng, T. T. Ising-traffic: Using ising machine learning to predict traffic congestion under uncertainty. In *Proceedings of the AAAI Conference on Artificial Intelligence*, 2023.
- Pierangeli, D., Marcucci, G., and Conti, C. Large-scale photonic ising machine by spatial light modulation. *Physical review letters*, 122(21):213902, 2019.
- Pumsirirat, A. and Yan, L. Credit card fraud detection using deep learning based on auto-encoder and restricted boltzmann machine. *International Journal of Advanced Computer Science and Applications*, 9(1), 2018. doi: 10.14569/IJACSA.2018.090103.
- Salakhutdinov, R. and Hinton, G. Deep boltzmann machines. In *Artificial intelligence and statistics*, pp. 448–455. PMLR, 2009.
- Salakhutdinov, R. and Murray, I. On the quantitative analysis of deep belief networks. In *Proceedings of the 25th international conference on Machine learning*, pp. 872–879, 2008.
- Salakhutdinov, R., Mnih, A., and Hinton, G. Restricted boltzmann machines for collaborative filtering. In *Proceedings of the 24th international conference on Machine learning*, pp. 791–798, 2007.
- Srivastava, N., Salakhutdinov, R. R., and Hinton, G. E. Modeling documents with deep boltzmann machines. *arXiv:1309.6865*, 2013.

- Takata, K., Marandi, A., Hamerly, R., Haribara, Y., Maruo, D., Tamate, S., Sakaguchi, H., Utsunomiya, S., and Yamamoto, Y. A 16-bit coherent ising machine for one-dimensional ring and cubic graph problems. *Scientific Reports*, 6(1):34089, 2016. doi: 10.1038/srep34089.
- Takeda, Y., Tamate, S., Yamamoto, Y., Takesue, H., Inagaki, T., and Utsunomiya, S. Boltzmann sampling for an XY model using a non-degenerate optical parametric oscillator network. *Quantum Science and Technology*, 3(1):014004, nov 2017. doi: 10.1088/2058-9565/aa923b.
- Verma, S., Patel, P., and Majumdar, A. Collaborative filtering with label consistent restricted boltzmann machine. In *2017 Ninth International Conference on Advances in Pattern Recognition (ICAPR)*, pp. 1–6. IEEE, 2017.
- Wang, H., Cai, Y., and Chen, L. A vehicle detection algorithm based on deep belief network. *The scientific world journal*, 2014, 2014.
- Wang, Y., Li, Y., Song, Y., and Rong, X. The application of a hybrid transfer algorithm based on a convolutional neural network model and an improved convolution restricted boltzmann machine model in facial expression recognition. *IEEE Access*, 7:184599–184610, 2019.
- Wang, Y., Pan, Z., Yuan, X., Yang, C., and Gui, W. A novel deep learning based fault diagnosis approach for chemical process with extended deep belief network. *ISA transactions*, 96:457–467, 2020.
- Xiao, H., Rasul, K., and Vollgraf, R. Fashion-mnist: a novel image dataset for benchmarking machine learning algorithms. *arXiv:1708.07747*, 2017.
- Xie, J., Du, G., Shen, C., Chen, N., Chen, L., and Zhu, Z. An end-to-end model based on improved adaptive deep belief network and its application to bearing fault diagnosis. *IEEE Access*, 6:63584–63596, 2018.
- Yamamoto, Y., Aihara, K., Leleu, T., Kawarabayashi, K.-i., Kako, S., Fejer, M., Inoue, K., and Takesue, H. Coherent ising machines—optical neural networks operating at the quantum limit. *npj Quantum Information*, 3(1):1–15, 2017.
- Yamaoka, M., Yoshimura, C., Hayashi, M., Okuyama, T., Aoki, H., and Mizuno, H. A 20k-spin ising chip to solve combinatorial optimization problems with cmos annealing. *IEEE Journal of Solid-State Circuits*, 51(1):303–309, 2015.
- Zames, G., Ajlouni, N., Ajlouni, N., Ajlouni, N., Holland, J., Hills, W., and Goldberg, D. Genetic algorithms in search, optimization and machine learning. *Information Technology Journal*, 3(1):301–302, 1981.
- Zhang, Q., Xiao, Y., Dai, W., Suo, J., Wang, C., Shi, J., and Zheng, H. Deep learning based classification of breast tumors with shear-wave elastography. *Ultrasonics*, 72:150–157, 2016.
- Zhao, Z., Xu, T., and Dai, C. Classifying images using restricted boltzmann machines and convolutional neural networks. In *Ninth International Conference on Digital Image Processing (ICDIP 2017)*, volume 10420, pp. 104202U. International Society for Optics and Photonics, 2017.